Large Eddy Simulation of a Gas Turbine Model Combustor using the Eulerian Subgrid Probability Density Function Method

D. Fredrich*, S. Gallot-Lavallée, W. P. Jones, A. J. Marquis
Department of Mechanical Engineering, Imperial College London, London, UK

Abstract
The Eulerian stochastic field method is applied to solve the subgrid Probability Density Function (PDF) accounting for turbulence-chemistry interaction in the Large Eddy Simulation (LES) of a swirl stabilised gas turbine model combustor. A dynamic version of the Smagorinsky model for the subgrid scale stresses and a gradient diffusion approximation for the scalar fluxes complete the formulation. The chemical reaction is described by a 15-step reduced CH_4 mechanism involving 19 species. Velocity, temperature and species results as well as basic thermochemical properties are shown to be in good agreement with experimental data validating the capabilities of the employed LES method.

Introduction

High levels of turbulence, fast chemical reactions and sophisticated geometrical features impede a deeper understanding of the complex flow physics in modern gas turbine combustors. A potentially powerful numerical tool capable of providing better insights into some of the physical processes encountered in these devices is Large Eddy Simulation (LES). The concept behind LES methods is to directly compute large-scale, energetic turbulent motions while the effects of motions whose 'size' is smaller than a defined filter width are modelled. One of the main challenges in the development of such methods for turbulent combustion is the interaction between turbulence and chemistry on the small, unresolved subfilter - or subgrid - scales. Governed by highly non-linear chemical reaction rates, turbulence-chemistry interaction appears in the form of a filtered chemical source term in the LES scalar equations and requires extensive modelling work. Various combustion models addressing the closure problem have been proposed in the past, though most of them formulated for one specific flame regime only. An overview of the different modelling techniques can be found, amongst others, in a review by Pitsch [1].

The subgrid combustion model underlying this work is based on a transported Probability Density Function (PDF) approach. It comes with the advantage of a regime independant description of turbulent flames, which becomes particularly useful in the context of gas turbine combustion. State of the art combustors are designed to operate under lean partially premixed conditions in order to effectively reduce pollutant emissions such as Nitrogen Oxides (NO_x) and Carbon monOxide (CO). In the partially premixed flame regime, parts of the flow field are governed by premixed flame propagation and finite-rate effects, i.e. ignition or extinction, while other parts will display mixing controlled reactions as encountered in diffusion (non-premixed) flames. It has been shown in the past that it is possible to capture these phenomena within a single LES framework by introducing the present fully Eulerian subgrid PDF approach to account for turbulence-chemistry interaction [2–4]. Bulat et al. [5, 6] have successfully applied the method to an industrial gas turbine combustor and achieved a good reproduction of the flow field. Local extinction of the flame was shown to be due to turbulence-chemistry effects rather than large-scale mixing and the combustor was found to have regions of diffusion flame regimes. Furthermore, it was found that the inclusion of radiative heat transfer has a notable influence on the flame location and leads to an improved prediction of the temperature field and species distribution.

Specific Objectives

The objective of the present work is to assess the predictive capabilities of the employed LES method in the context of partially premixed combustion in a complex geometry. For this purpose, test cases with varying mesh sizes are simulated and results are compared against available experimental data. This includes a characterisation of the flow field using mean axial and radial velocity component profiles at different locations in the combustion chamber as well as a description of the flame shape and location on the basis of both mean and Root Mean Square (RMS) temperature and CH_4 (methane) profiles. Moreover, the representation of fundamental thermochemical properties is evaluated by analysis of the instantaneous temperature-mixture fraction relation.

Mathematical Formulation

In LES the separation of large- and small-scale turbulent motions is achieved through a spatial filtering operation over the entire flow domain Ω. The spatial filter of a function $f = f(\mathbf{x}, t)$ is defined as its convolution with a filter function G according to:

$$\overline{f}(\mathbf{x}, t) = \int_{\Omega} G(\mathbf{x} - \mathbf{x}'; \Delta(\mathbf{x})) f(\mathbf{x}', t) \mathrm{d}\mathbf{x}' \qquad (1)$$

where the filter width Δ is taken to be the cube root of the local grid cell volume. In order to account for the strong density variations arising in combusting flows, additional density weighted - or Favre - filtering defined by $\widetilde{f} = \overline{\rho f}/\overline{\rho}$ can be introduced. Application of this filter to the equations of motion, i.e. mass conservation (2) and

*Corresponding author: d.fredrich15@imperial.ac.uk

momentum conservation (3), and to the scalar transport equations (4) results in the following set of filtered equations:

$$\frac{\partial \overline{\rho}}{\partial t} + \frac{\partial \overline{\rho}\widetilde{u}_i}{\partial x_i} = 0 \tag{2}$$

$$\frac{\partial \overline{\rho}\widetilde{u}_i}{\partial t} + \frac{\partial \overline{\rho}\widetilde{u}_i\widetilde{u}_j}{\partial x_j} = -\frac{\partial \overline{p}}{\partial x_i} + \frac{\partial}{\partial x_j}\left(2\mu\widetilde{S}_{ij}\right) - \frac{\partial \tau_{ij}^{sgs}}{\partial x_j} \tag{3}$$

$$\frac{\partial \overline{\rho}\widetilde{\phi}_\alpha}{\partial t} + \frac{\partial \overline{\rho}\widetilde{u}_j\widetilde{\phi}_\alpha}{\partial x_j} = \frac{\partial}{\partial x_j}\left(\frac{\overline{\mu}}{\sigma}\frac{\partial \widetilde{\phi}_\alpha}{\partial x_j}\right) - \frac{\partial J_{\alpha,j}^{sgs}}{\partial x_j} + \overline{\rho\dot{\omega}}_\alpha \tag{4}$$

The subgrid scale stress tensor $\tau_{ij}^{sgs} = \overline{\rho}\left(\widetilde{u_i u_j} - \widetilde{u}_i\widetilde{u}_j\right)$ is determined via the Smagorinsky model [7], which introduces a subgrid scale viscosity to mimic the diffusion process on the dissipative small-scales:

$$\mu_{sgs} = \overline{\rho}(C_s\Delta)^2||\widetilde{S}_{ij}|| \tag{5}$$

where $\widetilde{S}_{ij} = \frac{1}{2}\left(\frac{\partial \widetilde{u}_i}{\partial x_j} + \frac{\partial \widetilde{u}_j}{\partial x_i}\right)$ and $||\widetilde{S}_{ij}|| \equiv \sqrt{2\widetilde{S}_{ij}\widetilde{S}_{ij}}$ are the resolved rate of strain tensor and its respective Frobenius norm. The Smagorinsky parameter C_s is obtained through the dynamic procedure of Piomelli and Liu [8]. The isotropic part of the viscous and subgrid scale stresses is absorbed into the pressure. The scalar transport equations (4) are expressed in terms of a general scalar $\phi_\alpha = [\phi_1, ..., \phi_{N_s}]$ representing the species mass fractions Y_α and the enthalpy h where N_s is the number of scalars (number of species considered plus enthalpy) required to describe the system. Lewis number unity, low-Mach-number flow, constant thermodynamic pressure and equal diffusivities for all species ($D_\alpha = D$), which can be related to the viscosity via the Schmidt number $\sigma = \mu/\rho D$, have been assumed in the formulation. A gradient diffusion approximation is adopted for the scalar fluxes $J_{\alpha,j}^{sgs}$. The filtered chemical source term $\overline{\rho\dot{\omega}}_\alpha$ representing the net rate of species formation through chemical reaction remains unclosed and requires modelling.

The combustion model underlying the present work is a fully Eulerian transported subgrid PDF approach. Following Gao and O'Brien [9] and through the application of Favre filtering a joint subgrid PDF can be derived according to:

$$\widetilde{P}_{sgs}(\underline{\psi}; \mathbf{x}, t) = \frac{1}{\overline{\rho}}\int_\Omega \rho G(\mathbf{x} - \mathbf{x}', \Delta(\mathbf{x}))F(\underline{\psi}; \mathbf{x}', t)\mathrm{d}\mathbf{x}' \tag{6}$$

Here, F denotes the joint PDF, which is the product of the fine-grained probability density function P_α of each scalar:

$$F(\underline{\psi}; \mathbf{x}, t) = \prod_{\alpha=1}^{N_s} P_\alpha = \prod_{\alpha=1}^{N_s} \delta\left[\psi_\alpha - \phi_\alpha(\mathbf{x}, t)\right] \tag{7}$$

where ψ_α is the sample - or composition - space of the reactive scalar ϕ_α and δ is the Dirac-function. An exact equation describing the evolution of $\widetilde{P}_{sgs}$ can be derived from the appropriate conservation equations using standard methods, e.g. [9]. This formulation contains the chemical reaction term (I), which appears in closed form, as well as two additional unknown terms representing subgrid scale convection (II) and molecular diffusion (III) of the PDF. In the present work, these unknown terms are approximated, respectively, by a gradient closure directly analogous to the LES Smagorinsky model and by the Linear Mean Square Estimation (LMSE) closure [10], yielding the subgrid PDF evolution equation in its final form:

$$\begin{aligned}
&\overline{\rho}\frac{\partial \widetilde{P}_{sgs}(\underline{\psi})}{\partial t} + \overline{\rho}\widetilde{u}_j\frac{\partial \widetilde{P}_{sgs}(\underline{\psi})}{\partial x_j} = \\
&\underbrace{+\sum_{\alpha=1}^{N_s}\frac{\partial}{\partial \psi_\alpha}\left[\overline{\rho}\dot{\omega}_\alpha(\underline{\psi})\widetilde{P}_{sgs}(\underline{\psi})\right]}_{\textbf{I:}\ \text{closed chemical reaction term}} \\
&\underbrace{+\frac{\partial}{\partial x_j}\left[\left(\frac{\mu}{\sigma} + \frac{\mu_{sgs}}{\sigma_{sgs}}\right)\frac{\partial \widetilde{P}_{sgs}(\underline{\psi})}{\partial x_j}\right]}_{\textbf{II:}\ \text{sgs convection term (gradient closure)}} \\
&\underbrace{-\frac{\overline{\rho}}{2\tau_{sgs}}\sum_{\alpha=1}^{N_s}\frac{\partial}{\partial \psi_\alpha}\left[(\psi_\alpha - \widetilde{\phi}_\alpha(\mathbf{x}, t))\widetilde{P}_{sgs}(\underline{\psi})\right]}_{\textbf{III:}\ \text{molecular diffusion term (LMSE closure)}}
\end{aligned} \tag{8}$$

Here, the value 0.7 is assigned to the subgrid - or turbulent - Schmidt number σ_{sgs}. The micro-mixing time scale τ_{sgs} is assumed to be [11] given by:

$$\frac{1}{\tau_{sgs}} = C_d\frac{\mu + \mu_{sgs}}{\overline{\rho}\Delta^2} \tag{9}$$

where C_d is a micro-mixing constant with the value 2.0. The subgrid PDF evolution equation (8) is solved using the Eulerian stochastic field method, where $\widetilde{P}_{sgs}(\underline{\psi})$ is represented by an ensemble of N stochastic fields for each of the N_s scalars, namely $\xi_\alpha^n(\mathbf{x}, t)$. The joint subgrid PDF equation (6) can then be rewritten as follows:

$$\begin{aligned}
\widetilde{P}_{sgs}(\underline{\psi}; \mathbf{x}, t) = \frac{1}{N}\sum_{n=1}^{N}\frac{1}{\overline{\rho}}\int_\Omega \rho G(\mathbf{x} - \mathbf{x}', \Delta(\mathbf{x})) \\
\times \prod_{\alpha=1}^{N_s}\delta\left[\psi_\alpha - \xi_\alpha^n(\mathbf{x}, t)\right]\mathrm{d}\mathbf{x}'
\end{aligned} \tag{10}$$

In the present work, the Itô formulation is adopted for the stochastic integral [12] and the stochastic fields thus evolve according to:

$$\begin{aligned}
\overline{\rho}\mathrm{d}\xi_\alpha^n + \overline{\rho}\widetilde{u}_i\frac{\partial \xi_\alpha^n}{\partial x_i}\mathrm{d}t = \overline{\rho}\dot{\omega}_\alpha^n(\underline{\xi}^n)\mathrm{d}t + \frac{\partial}{\partial x_i}\left[\Gamma'\frac{\partial \xi_\alpha^n}{\partial x_i}\right]\mathrm{d}t \\
-\frac{\overline{\rho}}{2\tau_{sgs}}\left(\xi_\alpha^n - \widetilde{\phi}_\alpha\right)\mathrm{d}t + \overline{\rho}\sqrt{\frac{2\Gamma'}{\overline{\rho}}}\frac{\partial \xi_\alpha^n}{\partial x_i}\mathrm{d}W_i^n
\end{aligned} \tag{11}$$

where $\Gamma' = \frac{\mu}{\sigma} + \frac{\mu_{sgs}}{\sigma_{sgs}}$ is the total diffusion coefficient and $\mathrm{d}W_i^n$ represents increments of a vector Wiener process,

different for each field but independent of the spatial location **x**. The Favre filtered value of the reactive scalar ϕ_α can finally be obtained from averaging over the stochastic fields:

$$\widetilde{\phi}_\alpha = \frac{1}{N}\sum_{n=1}^{N} \xi_\alpha^n \qquad (12)$$

Experimental and Numerical Setup

The industrial model combustor considered in this work was experimentally investigated by Meier et al. [13] at DLR (German Aerospace Center) Stuttgart and Berlin as part of the PRECCINSTA (Prediction and Control of Combustion Instabilities in Industrial Gas Turbines) project. Its radial swirler is based on a Turbomeca design and representative of industrial gas turbine combustion. The combustor geometry is schematically depicted in Fig. 1 and comprises four sections. In the first section, dry, pure air at atmospheric conditions is fed into the plenum through a large orifice. The second section consists of the radial swirler followed by a bluff body. In between each of the 12 swirler vanes, a 1 mm diameter fuel hole injects methane into the air stream with high momentum to ensure good mixing. The resulting mixture, with an overall equivalence ratio of $\Phi = 0.7$, swirls around the bluff body before entering the combustion chamber section made of 1.5 mm thick quartz glass windows providing optical access on each side. The chamber entry plane - aligned with the bluff body tip - is defined as axial location $h_0 = 0$ for all measurements. Comprehensive experimental data is available from Laser Doppler Velocimetry (LDV) and laser Raman scattering measurements. These provide both mean and RMS values of the velocity, temperature, mixture fraction and species concentration. Measurements were performed in one vertical plane along radial profiles at different axial locations within the combustion chamber. The systematic and statistical uncertainties are, respectively, less than 0.5% and ±1.5-2% for the velocity components, ±3-4% and ±2.5% for the temperature, ±3-4% and ±1% for the mixture fraction and +5-9% and ±1-3% for the CH_4 mole fraction. The burnt combustion products eventually exit the domain through the fourth section connecting the combustor to the atmosphere via a converging duct.

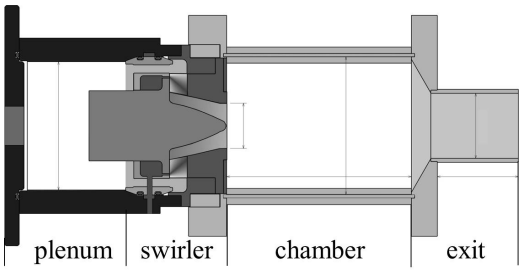


Figure 1: Schematic [13] of the PRECCINSTA combustor. The combustion chamber has a 85 x 85 mm^2 cross section area and an axial length of h = 114 mm.

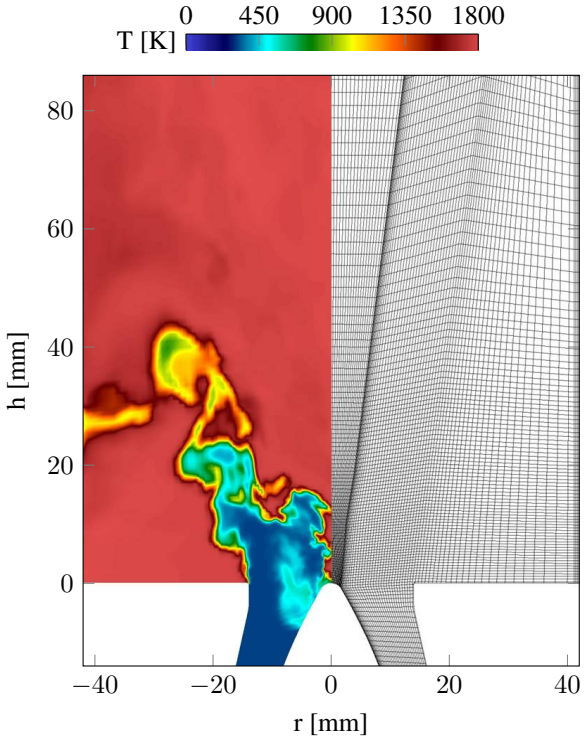


Figure 2: Snapshot of the instantaneous temperature field obtained from the fine mesh LES (left) and flame region close-up of the computational fine mesh (right).

The in-house, block-structured, boundary conforming coordinate LES code BOFFIN-LES is employed for all the computations. It is fully parallelised by means of domain decomposition and MPI message passing routines. The code utilises a second-order-accurate finite volume method, based on a fully implicit low-Mach-number, pressure based, variable density formulation. For the momentum equation convection terms, an energy-conserving discretisation scheme is used. All other spatial derivatives are discretised with second-order central differences, with the exception of the convective terms in the scalar equations. These are discretised using a Total Variation Diminishing (TVD) scheme to avoid unphysical overshoots. A description of the weak first-order temporal approximation used for solving the stochastic field equations can be found in [14]. The chemistry is represented by a 15-step Augmented Reduced Mechanism (ARM), which was derived by Sung et al. [15] from the full GRI 3.0 mechanism and involves 19 species. For the simulations, one stochastic field is used to characterise the influence of the subgrid scale contributions. The computational domain is equivalent to the combustor geometry investigated in the experimental test campaign. Two block-structured meshes were created containing ∼2.7 million cells (fine mesh; depicted in Fig. 2) and ∼0.5 million cells (coarse mesh). In order to account for preheating of the mixture before it enters the combustion chamber, as observed in the experiments [13], both air and methane are injected at a temperature of 320 K

and a pressure of 1 bar. The inlet velocities were adjusted accordingly to reflect the prescribed mass flow rates. A zero-gradient pressure boundary condition is adopted for the outlet plane and all of the domain walls are treated as adiabatic. Radiative heat transfer is considered in the simulations through a radiation model described in [16].

Results and Discussion

Radial profiles of the mean axial and radial velocity components at five different axial locations h downstream of the bluff body are presented in Fig. 3. Results from the LDV measurements are identified by diamonds whereas fine and coarse mesh LES results are plotted as solid black and dashed green lines, respectively. When characterising the flow field, three distinctive flow regions can be identified. An Inner Recirculation Zone (IRZ), created by the swirling flow to stabilise the flame, can easily be detected due to the high negative velocities around the combustor centreline. The conically shaped, swirling jet of unburnt gases is characterised by high axial velocity values peaking at 40 m/s and high radial velocity magnitudes reaching approximately 20 m/s. Lower velocities towards the combustion chamber walls indicate the transition into an Outer Recirculation Zone (ORZ), which is located outside of the experimentally measured region. With increasing downstream position, the high velocity jet widens and shifts towards the combustion chamber walls reducing the size of the ORZ while widening the IRZ. All of the above flow characteristics are captured by the LES. Solely the coarse mesh solution has difficulties reproducing the high negative axial velocities in the IRZ and the radial velocities close to chamber walls at downstream locations h_{15} and h_{25}. The fine mesh velocity results match the experimental data with a very high accuracy and show a marginally better overall agreement compared to the coarse mesh results.

Figure 4 shows radial profiles of the mean and RMS temperature for different axial locations in the combustor. A corresponding instantaneous snapshot of the fine mesh temperature field is presented in Fig. 2 illustrating the highly turbulent flame behaviour. Looking at the mean profiles, general temperature trends including the location of the temperature dip representing unburnt gases are well reproduced by the LES. Nonetheless, a shortened simulated flame length can be determined as the temperature values converge towards their equilibrium state - with downstream position - at a quicker rate. The small number of stochastic fields utilised in the calculation of the PDF evolution equation can be identified as a potential cause for this. Previous findings by Jones et al. [2] (or e.g. [17]) suggest that eight stochastic fields provide a reasonable compromise between prediction quality and computational costs. However, due to limited computational resources, only one stochastic field has been used in this work. At h_{80} both the experimental and numerical temperatures reach an equlibrium state at the adiabatic flame temperature of just over 1800 K. RMS temperature profiles are plotted on the right-hand side of Fig. 4 and

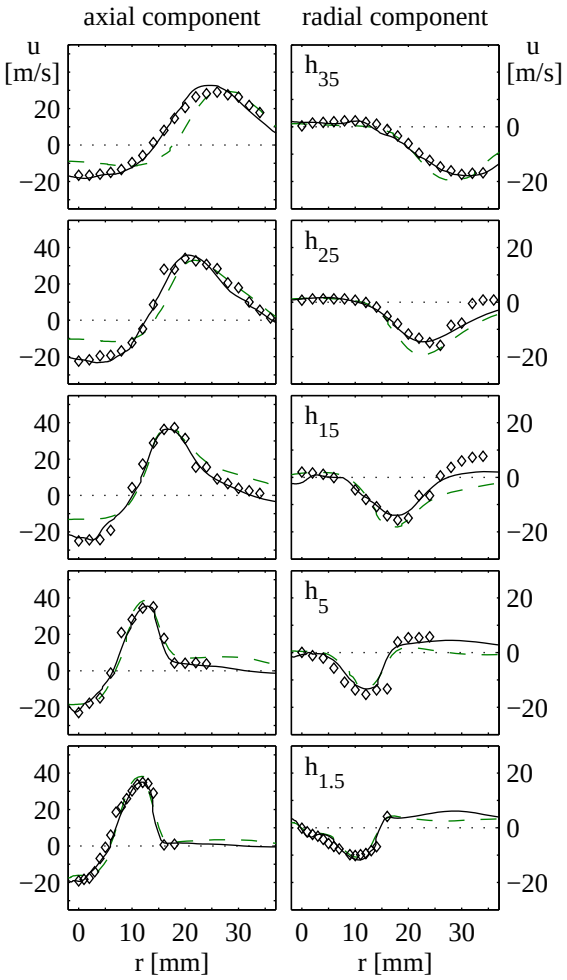


Figure 3: Radial profiles of mean axial (left) and radial (right) velocity components from the experiments (◇), fine mesh LES (−) and coarse mesh LES (− −) at axial locations h = 1.5, 5, 15, 25, 35 mm.

it becomes clear that the RMS values are consistently underestimated towards the combustor centreline. The method's incapabilty to reproduce an oscillating flame undergoing self-excited thermo-acoustic instabilities (observed in the experiments [13]) may serve as a possible reason for the underestimation. In a previous LES of the same combustor, Franzelli et al. [18] have shown a significant improvement of RMS temperature results close to the centreline by resolving flame oscillations. Despite this shortcoming, all of the RMS temperature profiles are accurately reproduced away from the centreline. Finally, it can be noted that the fine mesh is capable of providing a slightly better overall description of the flame shape and location.

Radial profiles of both the mean and RMS CH_4 mass fraction are depicted in Fig. 5. The mean profiles suggest an earlier (further upstream) consumption of methane at axial locations h_6 to h_{30}, which is consistent with the above mean temperature results displaying a shortened flame length. At h_{80}, all of the methane is fully con-

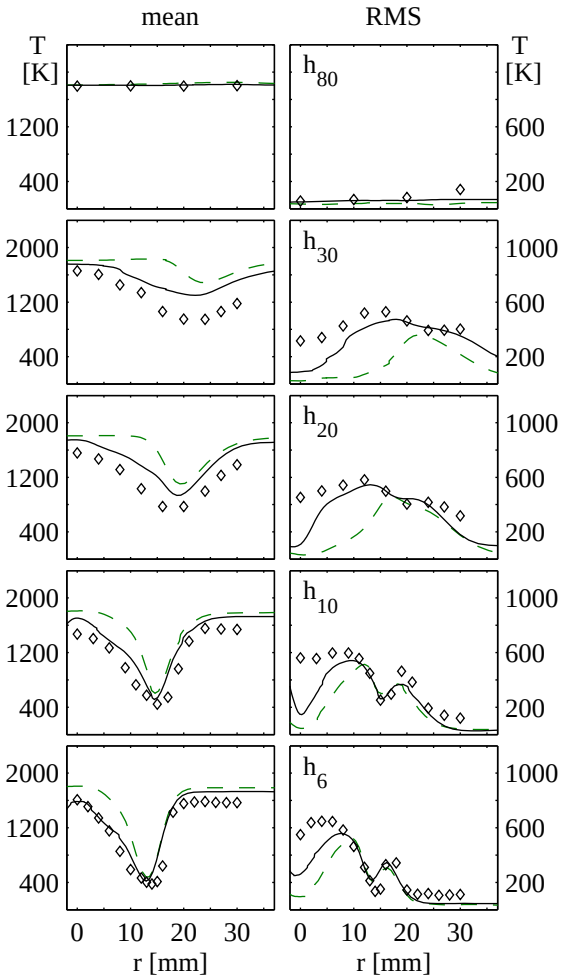


Figure 4: Radial profiles of mean (left) and RMS (right) temperatures from the experiments (◇), fine mesh LES (−) and coarse mesh LES (− −) at axial locations h = 6, 10, 20, 30, 60 mm.

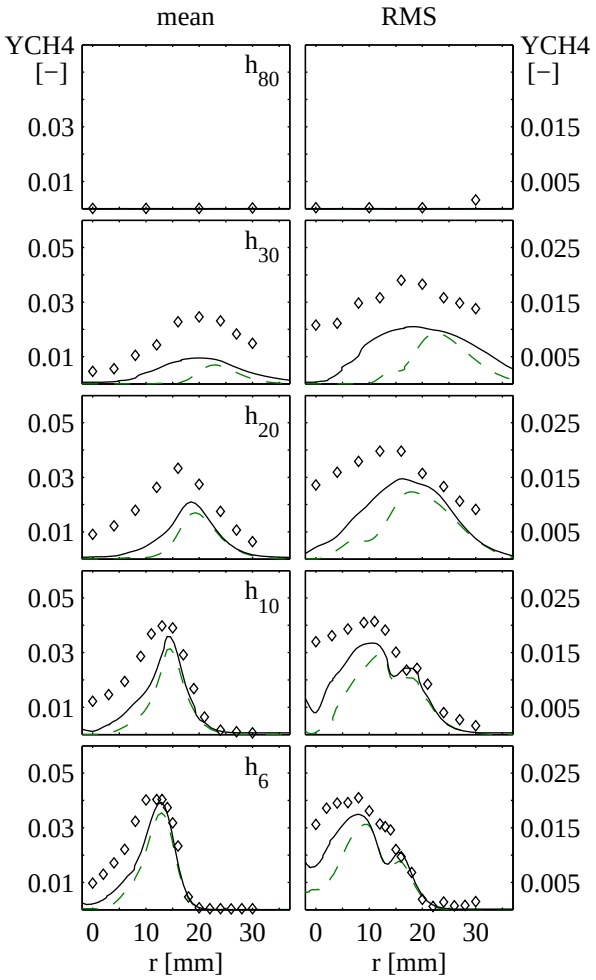


Figure 5: Radial profiles of mean (left) and RMS (right) CH_4 mass fractions from the experiments (◇), fine mesh LES (−) and coarse mesh LES (− −) at axial locations h = 6, 10, 20, 30, 60 mm.

sumed as expected from comparisons with the experimental measurements. In accordance with the RMS temperature profiles, the RMS values of CH_4 are not fully captured in the LES particularly towards the centreline of the combustor, however, a decent description of the general RMS trends can be concluded. Again, comparing the coarse and fine mesh solutions, results obtained from the fine mesh are in better agreement with experimental data.

The numerically predicted thermochemistry can be analysed in terms of the instantaneous relation between temperature and mixture fraction as shown in Fig. 6 for four axial locations in the combustor. Each scatter on the left-hand side of the figure represents one experimental single-shot laser Raman scattering measurement taken at different radial positions over time. LES results, obtained at identical locations, are plotted on the right-hand side. Looking at the evolution of the simulated temperature-mixture fraction distribution with downstream location, the shortened flame length determined in the above mean temperature and CH_4 mass fraction results can be observed once again. Unlike the experimental findings at axial location h_6, only a small amount of scatters is located within the fresh gas region below approximately 400 K. Furthermore, at h_{15}, all of the scatters have moved up into either the reaction zone with intermediate temperatures or the fully burnt region close to the solid line, which represents the calculated adiabatic flame temperature. Finally, looking at the mixture fraction distributions, experimental extreme values of about $Z_{min} \approx 0.015$ and $Z_{max} \approx 0.08$ can be observed. It becomes clear that the LES does not reproduce such wide range of mixture fraction values but instead predicts a higher degree of premixing. The expanded experimental distribution is likely to be caused by the occurrence of thermo-acoustic instabilities periodically varying the amount of fuel in the mixture, as observed experimentally by Meier et al. [13] and numerically by Franzelli et al. [18]. Overall, the simulated scatterplots of the instantaneous temperature-mixture fraction relation match experimental results and the mixture fraction distribution is adequately estimated.

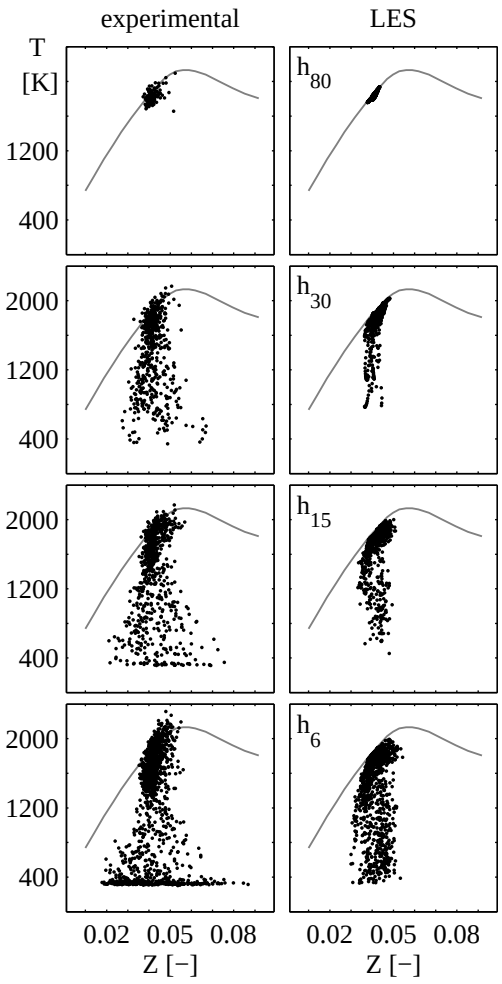


Figure 6: Instantaneous scatter plots of temperature versus mixture fraction from the experiments (left) and fine mesh LES (right) at axial locations h = 6, 15, 30, 80 mm. The adiabatic flame temperature is indicated by a solid line and the global mixture fraction is $Z_{global} = 0.0391$.

Conclusions

The PRECCINSTA gas turbine model combustor was successfully simulated using LES in conjunction with the Eulerian subgrid PDF combustion model. The flow field was found to be in excellent agreement with experimental data supporting the suitability of the solver with a dynamic subgrid turbulence model to highly swirling flows. In contrast to the velocity field, the scalar fields showed a noticeable dependency on the mesh resolution with the fine mesh providing a slightly better description of the flame shape and location. Temperature and species mass fraction profiles as well as the basic thermochemical properties were generally well predicted validating the capabilities of the subgrid PDF approach. However, it has to be noted that the flame length was underestimated by the LES compared to experimental measurements, which could be attributed to the utilisation of only one stochastic field in the PDF calculation. In summary, the employed LES method has been validated for partially premixed combustion in a complex geometry. Subsequent simulations with a larger number of stochastic fields will show if further improvement of the results can be achieved. A future extension of the method to compressible flow may allow for the reproduction of thermo-acoustic instabilities observed in the experiments.

Acknowledgements

The authors are grateful to SIEMENS Industrial Turbomachinery Ltd. for their financial support. This work used the ARCHER UK National Supercomputing Service (http://www.archer.ac.uk).

References

[1] H. Pitsch. Annual Review of Fluid Mechanics 38 (1) (2006), 453–482.
[2] W. P. Jones and S. Navarro-Martinez. Combustion and Flame 150 (3) (2007), 170–187.
[3] W. P. Jones and V. N. Prasad. Combustion and Flame 157 (9) (2010), 1621–1636.
[4] W. P. Jones and V. N. Prasad. Proceedings of the Combustion Institute 33 (1) (2011), 1355–1363.
[5] G. Bulat, W. Jones, and A. Marquis. Proceedings of the Combustion Institute 34 (2) (2013), 3155–3164.
[6] G. Bulat, W. P. Jones, and A. J. Marquis. Combustion and Flame 161 (7) (2014), 1804–1825.
[7] J. Smagorinsky. Monthly Weather Review 91 (3) (1963), 99–164.
[8] U. Piomelli and L. Junhui. Physics of Fluids 7 (4) (1995), 839–848.
[9] F. Gao and E. E. O'Brien. Physics of Fluids A: Fluid Dynamics 5 (6) (1993), 1282–1284.
[10] C. Dopazo and E. O'Brien. The Physics of Fluids 17 (11) (1974), 1968–1975.
[11] W. P. Jones and M. Kakhi. Combustion and Flame 115 (1-2) (1998), 210–229.
[12] L. Valiño. Flow, Turbulence and Combustion 60 (2) (1998), 157–172.
[13] W. Meier, P. Weigand, X. R. Duan, and R. Giezendanner-Thoben. Combustion and Flame 150 (1-2) (2007), 2–26.
[14] R. Mustata, L. Valiño, C. Jimenez, W. P. Jones, and S. Bondi. Combustion and Flame 145 (1-2) (2006), 88–104.
[15] C. J. Sung, C. K. Law, and J. Y. Chen. Combustion and Flame 125 (1-2) (2001), 906–919.
[16] R. S. Barlow, A. N. Karpetis, J. H. Frank, and J. Y. Chen. Combustion and Flame 127 (3) (2001), 2102–2118.
[17] S. Gallot-Lavallée and W. P. Jones. Flow, Turbulence and Combustion 96 (2) (2016), 513–534.
[18] B. Franzelli, E. Riber, L. Y. M. Gicquel, and T. Poinsot. Combustion and Flame 159 (2) (2012), 621–637.